

Accelerating AIGC Services with Latent Action Diffusion Scheduling in Edge Networks

Changfu Xu, *Student Member, IEEE*, Jianxiong Guo, *Member, IEEE*, Wanyu Lin, *Member, IEEE*, Haodong Zou, *Student Member, IEEE*, Wentao Fan, *Senior Member, IEEE*, Tian Wang, *Senior Member, IEEE*, Xiaowen Chu, *Fellow, IEEE*, and Jiannong Cao, *Fellow, IEEE*

Abstract—Artificial Intelligence Generated Content (AIGC) has gained significant popularity for creating diverse content. Current AIGC models primarily focus on content quality within a centralized framework, resulting in a high service delay and negative user experiences. However, not only does the workload of an AIGC task depend on the AIGC model’s complexity rather than the amount of data, but the large model and its multi-layer encoder structure also result in a huge demand for computational and memory resources. These unique characteristics pose new challenges in its modeling, deployment, and scheduling at edge networks. Thus, we model an offloading problem among edges for providing real AIGC services and propose LAD-TS, a novel Latent Action Diffusion-based Task Scheduling method that orchestrates multiple edge servers for expedited AIGC services. The LAD-TS generates a near-optimal offloading decision by leveraging the diffusion model’s conditional generation capability and the reinforcement learning’s environment interaction ability, thereby minimizing the service delays under multiple resource constraints. Meanwhile, a latent action diffusion strategy is designed to guide decision generation by utilizing historical action probability, enabling rapid achievement of near-optimal decisions. Furthermore, we develop DEdgeAI, a prototype edge system with a refined AIGC model deployment to implement and evaluate our LAD-TS method. DEdgeAI provides a real AIGC service for users, demonstrating up to 29.18% shorter service

delays than the current five representative AIGC platforms. We release our open-source code at <https://github.com/ChangfuXu/DEdgeAI>.

Index Terms—Edge computing, Diffusion scheduling, Accelerating AIGC service, Reinforcement learning

I. INTRODUCTION

The technique of Artificial Intelligence Generated Content (AIGC) has garnered substantial attention and demonstrated considerable success in today’s industrial applications [1]. The main aim of AIGC is to autonomously generate the corresponding human-aware content, such as text, images, and video, according to the instructions given by users. Due to the superior capacity of these content creations, the development of AIGC has become a prominent research hotspot [2].

In recent years, with the rise of ChatGPT [3], various AIGC models (such as Midjourney [4] and Sora [5]) are constantly being proposed [6]. For instance, by using Deep Reinforcement Learning (DRL) from human feedback, ChatGPT would generate the most appropriate response for a given instruction, improving the reliability and accuracy of its model [3]. However, current AIGC models focus on the quality performance of content generation and are predominantly operated by the Cloud Server (CS) within a centralized service framework, as shown in Fig. 1. This makes a high service response time for AIGC services, leading to a bad Quality of Experience (QoE) [2]. For example, users generally experience 40 – 80 seconds wait for image generation on platforms such as Midjourney [4] and Hugging Face [7]. Therefore, there is a pressing need for the QoE improvement of AIGC applications.

Fortunately, edge computing has emerged as a promising technology to provide lower service delay at Edge Servers (ESs) compared to traditional centralized cloud computing [8]–[13]. For instance, Xu *et al.* [14] propose a dynamic parallel multi-ES selection and workload allocation approach in collaborative edge computing systems. In these methods, some task workloads are locally processed at the ES, and some are offloaded to other ESs or the CS for processing [15]–[17]. As a result, the QoE for task requests in both ES and CS are improved. This motivates us to regard ESs as a resource pool to collaboratively process AIGC requests, thus improving AIGC applications’ QoE.

However, we observe some challenges to realizing AIGC services in edge networks. **First Challenge:** Different from traditional tasks, the AIGC task workload is mainly determined

This work was supported in part by grants from the National Natural Science Foundation of China (NSFC) (62172046, 62372047, 62202055), the Beijing Natural Science Foundation (No. 4232028), the Natural Science Foundation of Guangdong Province (2024A1515011323), Zhuhai Basic and Applied Basic Research Foundation (2220004002619), the Joint Project of Production, Teaching and Research of Zhuhai (2220004002686, 2320004002812), Science and Technology Projects of Social Development in Zhuhai (2320004000213), the Supplemental Funds for Major Scientific Research Projects of Beijing Normal University, Zhuhai (ZHPT2023002), the Fundamental Research Funds for the Central Universities, Higher Education Research Topics of Guangdong Association of Higher Education in the 14th Five-Year Plan under 24GYB207, Beijing Normal University Education Reform Project under jx2024139. (*Corresponding Author: Tian Wang.*)

Changfu Xu and Haodong Zou are with the BNU-HKBU United International College, Zhuhai 519087, China, and the Hong Kong Baptist University, Hong Kong. (E-mail: {changfuxu, haodongzou}@uic.edu.cn)

Jianxiong Guo is with the Institute of Artificial Intelligence and Future Networks, Beijing Normal University, Zhuhai 519087, China, and the Guangdong Key Lab of AI and Multi-Modal Data Processing, BNU-HKBU United International College, Zhuhai 519087, China. (E-mail: jianxiongguo@bnu.edu.cn)

Wentao Fan is with the BNU-HKBU United International College, Zhuhai 519087, China. (E-mail: wentaofan@uic.edu.cn)

Tian Wang is with the Institute of Artificial Intelligence and Future Networks, Beijing Normal University, Zhuhai 519087, China. (E-mail: tianwang@bnu.edu.cn)

Xiaowen Chu is with the Hong Kong University of Science and Technology (Guangzhou), Guangzhou, China. (E-mail: xwchu@hkust-gz.edu.cn)

Wanyu Lin and Jiannong Cao are with the Department of Computing, Hong Kong Polytechnic University, Hong Kong. (E-mail: {wanyulin, csj-cao@comp.polyu.edu.hk})

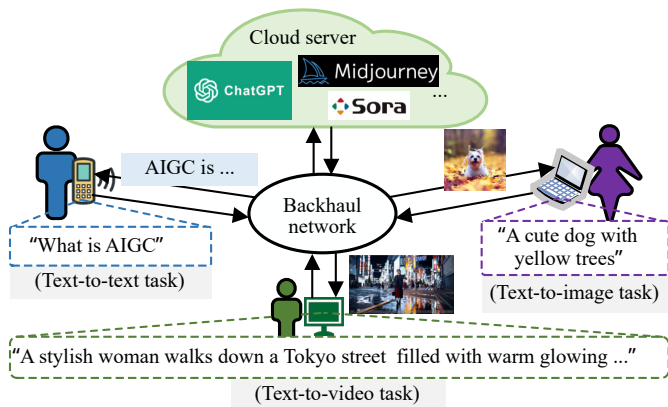


Figure 1. An illustration of existing AIGC applications. Users send their prompts to the cloud server that has deployed the corresponding AIGC models by backhaul network. Then, the corresponding contents (e.g., image) are generated according to the prompts and are sent back to users by the server.

by the self-complexity of the AIGC model rather than the size of task data. Moreover, different AIGC models have different network structures. All these pose a challenge in modeling AIGC tasks. **Second Challenge:** AIGC tasks are also computation-intensive due to the large parameters of AIGC model. Thus, when many AIGC tasks simultaneously arrive in the edge system, we have to schedule these tasks to other available ESs for parallel processing due to limited computing resources on local ES, ensuring a good QoE. However, the processing of task scheduling is an online decision-making problem, which makes it computationally infeasible to attain an optimal solution within polynomial time. In addition, although many DRL-based scheduling solutions have recently been proposed to reduce service delay, they have a low balance capability between exploration and exploitation. **Third Challenge:** AIGC services are usually large models and use several text encoders. For example, a classic AIGC model DALL-E [18] has 12 billion parameters. Another well-known AIGC model Stable Diffusion 3 (SD3) [19] has three pretrained text encoders—OpenCLIP-ViT/G, CLIP-ViT/L, and T5xxl—to encode text representations and an improved autoencoding model to encode image tokens. This makes the deployment of AIGC services require a large amount of memory. However, edge devices (e.g., Nvidia Jetson) have limited memory resource, which leads to a significant challenge in the real deployment of AIGC services on edge networks.

To address the above challenges, we propose **LAD-TS**, a novel Latent Action Diffusion-based Task Scheduling method that can orchestrate multiple ESs for expedited AIGC services. Furthermore, we develop **DEdgeAI**, a prototype edge system to implement and evaluate our LAD-TS method for real AIGC services. LAD-TS and DEdgeAI’s contributions go beyond leveraging distributed ESs to accelerate AIGC services and address the above challenges at three levels. Specifically, *in response to the first challenge*, by analyzing the feature of the AIGC model, we model the offloading problem among edges for providing real AIGC services and

formulate it as an online Integer Non-Linear Programming (INLP) problem with NP-hardness. The problem objective is designed to minimize the average delay of all task offloading in the system, ensuring the QoE of AIGC applications in edge networks. *For the second challenge*, we observe that since the diffusion model has guidance with exceptional conditions (e.g., text), the integration of the diffusion model and DRL techniques represents a complement to the balance between exploration and exploitation, thus broadening the effectiveness of decision optimization in dynamic edge environments. Thus, we propose the LAD-TS method to generate the approximate optimal offloading decisions by utilizing the diffusion model’s condition generation capability and the DRL’s environment interaction ability. As a result, LAD-TS can minimize service delays under multiple resource constraints. Meanwhile, by leveraging historical action probability instead of random Gaussian noise in the diffusion processing, we also design a latent action diffusion strategy to guide decision generation, which enables fast achievement of near-optimal decisions. Moreover, we provide a theoretical analysis to show the LAD-TS’s probability derivation. *To address the third challenge*, we develop the DEdgeAI to deploy a refined SD3 medium model, named **reSD3-m**, by removing T5xxl encoder. Furthermore, we implement the LAD-TS method in the DEdgeAI system to provide a real AIGC service at the edges. Finally, extensive evaluations and test-bed results show the effectiveness of our LAD-TS method and DEdgeAI system while reducing the memory occupation on the ESs significantly. This paper makes the following main contributions:

- **Modeling:** Unlike the existing task scheduling modeling in edge computing, we model the offloading problem among edges for real AIGC services and formulate it as an online INLP problem to minimize the average delay of all task offloading in the system. Moreover, we prove the NP-hardness of the offline counterpart of the problem.
- **Method:** We propose a novel LAD-TS method that utilizes multiple ESs for expedited AIGC services. Meanwhile, we optimize the task scheduling policy by designing a latent action diffusion strategy, achieving near-optimal decisions quickly. Furthermore, we implement our LAD-TS method as an online distributed algorithm with corresponding theoretical analysis, showing the LAD-TS’s probability derivation. Extensive simulation evaluations reveal that our LAD-TS method significantly reduces the service delay by 8.58% to 33.67% and the training episode duration by at least 60% compared to the state-of-the-art methods.
- **System:** We also develop the DEdgeAI system with the reSD3-m deployment on distributed edge devices to implement and evaluate our LAD-TS method. Test-bed results demonstrate that DEdgeAI achieves a service delay improvement of at least 29.18% compared to five representative AIGC platforms and a memory occupation reduction by about 60% compared to the original SD3 medium model.

Table I
COMPARISON OF OURS AND CURRENT REPRESENTATIVE METHODS

Method	Cloud-enabled AIGC	Edge-enabled AIGC	Diffusion scheduling	Latent action diffusion	Delay optimization
Midjourney [4]	✓	✗	✗	✗	✗
Xu <i>et al.</i> [24]	✗	✓	✗	✗	✓
Du <i>et al.</i> [25]	✗	✓	✓	✗	✗
Ours	✗	✓	✓	✓	✓

The remainder of this paper is organized as follows. Section II introduces the related work. Section III presents the system model and problem formulation. Section IV and Section V give the specific details and effectiveness evaluation of our method, respectively. The test-bed results and conclusion are shown in Section VI and Section VII, respectively.

II. RELATED WORK

In this section, we briefly review the related work of cloud-enabled AIGC, edge-enabled AIGC, and diffusion scheduling.

A. Cloud-enabled AIGC

A large amount of research currently focuses on cloud-enabled AIGC with a centralized framework, where AIGC services are primarily deployed on the CS for clients' usage [4], [20] (see in Fig. 1). For instance, in the ChatGPT [21] application, all users send their prompts to the CS for processing in a centralized way. Similarly, other AIGC applications, such as SD3 models [22] and VideoGPT [23], for generating images also use the resource in the CS to process all user requests. These applications have been widely studied due to their superior generation capabilities. However, they just adopt a centralized platform that has limited network bandwidths. Additionally, they also demand a huge computing capacity for the CS. Consequently, the response time for achieving processing results is usually high due to the long distance between users and the CS, especially for many user requests.

B. Edge-enabled AIGC

To reduce the service delay in cloud-enabled AIGC applications, the edge-enabled AIGC methods [2], [26] have been proposed to provide AIGC services at the network edge. By considering the rigid assumptions of traditional heuristic algorithms, current edge-enabled AIGC methods use DRL (e.g., [27], [28]) techniques to realize task scheduling as the DRL can optimize offloading decisions through interaction with the environment [29], [30]. For example, Xu *et al.* [24] propose an adaptive multi-server collaboration approach for edge-enabled AIGC based on DRL, thereby enhancing AIGC efficiency. These DRL-based methods can efficiently adapt to unforeseen changes in task characteristics due to their dynamic learning framework, making them highly suitable for scheduling challenges in real-time systems. However, DRL-based methods have a low balance capability between exploration and exploitation, which often results in suboptimal policies and diminished system QoS. Additionally, they also have an issue of low sample efficiency since they typically require

extensive interaction with the environment, leading to high computational costs and time consumption [31].

C. Diffusion Scheduling

Diffusion models have recently gained popularity in machine learning, particularly for applications such as image and video generation and molecular design [32]. In computer vision, diffusion-based neural networks generate images by reversing the diffusion process, which typically involves introducing Gaussian noise and then gradually removing it [19]. Recently, a combination of diffusion models and DRL has been explored for task scheduling in edge computing [33], [34]. For example, Du *et al.* [25] propose a Deep Diffusion-based Soft-Actor-Critic Task Scheduling (D2SACTS) algorithm that integrates diffusion models with DRL techniques to enhance decision optimization for task scheduling in edge computing systems. These methods learn decision policy by the combination of the diffusion model and the DRL technique, thereby enhancing the effectiveness of decision optimization. However, they fail to find the scheduling decision quickly and exhibit performance instability in complex edge environments since their diffusion processing is based on Gaussian noise.

D. Comparison Analysis

Table I summarizes the difference between current representative methods and our method. *First*, current AIGC methods, such as [4], [18], mainly are enabled by the CS with a centralized platform. Consequently, our method is enabled by ESs with a distributed AIGC service deployment, alleviating network bandwidth limitations. Meanwhile, our method performs task scheduling in a distributed way, avoiding scheduling congestion for large user requests. *Second*, although methods in [24] and [25] consider a distributed AIGC service deployment, they have a low balance capability between exploration and exploitation or consider the diffusion processing based on Gaussian noise. Moreover, the method in [25] adopts a centralized task scheduling without delay optimization, which cannot be applied to our problem directly. In contrast, our method implements diffusion processing by using a latent action diffusion strategy, thereby achieving near-optimal policy quickly. Additionally, our method performs the delay optimization for distributed AIGC services, ensuring low service delays for AIGC applications.

Table II
SYMBOLS FREQUENTLY USED IN THIS PAPER.

Symbol	Description
\mathcal{T}	The set of time slots.
\mathcal{B}	The set of ESs or BSs.
$\mathbb{N}_{b,t}$	The task set that arrives to BS $b \in \mathcal{B}$ at time slot $t \in \mathcal{T}$.
Δ	The length of each time slot $t \in \mathcal{T}$.
d_n	The data size of task $n \in \mathbb{N}_{b,t}$.
z_n	The generation quality demand of an AIGC task n .
ρ_n	The required computation density of offloading task n .
ψ	The decision variable of task scheduling decision.
v	The transmission rate between BSs
$f_{b'}$	The CPU or GPU computing capacity of ES $b' \in \mathcal{B}$
$T_{b,n,t,b'}^{\text{serv}}$	The service delay of offloading task n that is allocated from BS b to ES b' at time slot t .
$T_{b,n,t,b'}^{\text{wait}}$	The waiting time of task n in the transmission queue at local BS b and the processing queue at ES b' .
$q_{t,b'}$	The processing queue workload length of ES b' at the end of time slot $t - 1$.
$q_{n,t,b'}^{\text{bef}}$	The workload length of the processing queue at ES b' before receiving task n at time slot t .

III. SYSTEM MODEL AND PROBLEM FORMULATION

In this section, we first present the AIGC system model and then formally formulate our problem. Table II summarizes the notations frequently used in this paper.

A. AIGC System Model

We consider AIGC applications within a distributed edge system as illustrated in Fig. 2. The network consists of multiple Base Stations (BSs), each equipped with an ES. These ESs have different computing capacities and deploy different AIGC services, such as SD [19] and LLaMA [35] models. All BSs are connected via a wired core network. Each ES has a scheduler with a processing queue. The processing queue retains the tasks pending computation by the available CPU and GPU resources. Then, when AIGC tasks reach a BS within a given time slot, the BS' scheduler determines the allocation of task workloads to the appropriate ESs for parallel processing. Let $\mathcal{B} = \{1, \dots, B\}$ represent the set of ESs or BSs, with $b \in \mathcal{B}$ indicating the b -th ES and B denoting the total count of ESs. The system operates over consecutive time slots, denoted by $\mathcal{T} = \{1, \dots, |\mathcal{T}|\}$ [36], [37], where $t \in \mathcal{T}$ signifies the t -th time slot. We set the duration of each time slot $t \in \mathcal{T}$ to Δ seconds. In subsequent sections, we will elaborate on the AIGC task model, scheduling decision variable, and service delay model.

1) *AIGC Task Model*: We focus on the text-to-image and image-to-image tasks in AIGC applications. For convenience, we use the SD services as an AIGC service example for modeling. Notably, in the text-to-image task, each task's input is a piece of text and its corresponding demand of image quality. In contrast, the input of each image-to-image task has an image and the prompt of text description. Unlike general tasks, the workload of an AIGC task is typically not determined by its data size. To address this issue, we first let $\mathbb{N}_{b,t} = \{1, 2, \dots, N_{b,t}\}$ denote a set of AIGC tasks arrived to BS b at the same time slot t , where $n \in \mathbb{N}_{b,t}$ denotes as the

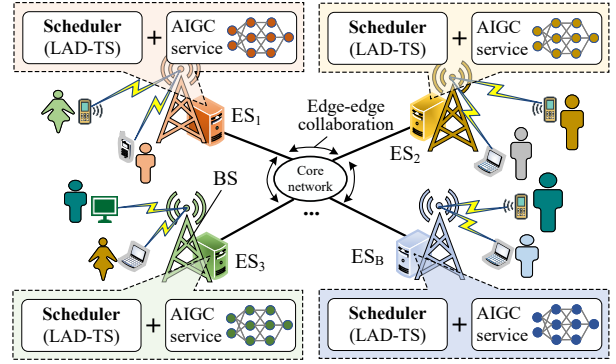


Figure 2. An illustration of the efficient distributed AIGC in this paper. For each AIGC task in each time slot, the scheduler will decide which ES to process the task by the proposed LAD-TS method.

n -th task. Then, for a specific text-to-image or image-to-image task n , we use a variable d_n (in bits) to represent the inputted data (text or text and image) size of task n . Furthermore, by analyzing the network structure of the SD model, we observe that the generating image quality relies on the number of denoising steps. In other words, the more denoising steps the better image generation. Thus, the number of denoising steps can well represent the demand for generating image quality in the SD model. Based on this observation, we define a variable z_n for the number of denoising steps and then the workload of the task n can be modeled as $\rho_n \cdot z_n$ (in CPU or GPU cycles if GPU is available). Here, ρ_n (in CPU cycles/step) is the required computing resources of each denoising step for task n and is determined by the task type, AIGC model types, and ES performance. Notably, our modeling method can be extended to other AIGC applications by changing partial formulation expressions according to specific task types.

2) *Scheduling Decision Variable*: Each task will be allocated to a suitable ES to generate an image for each time slot in our problem. Let a binary variable $\psi_{b,n,t,b'} \in \{0, 1\}$ denote the allocation decision of offloading task n from the BS b to the ES $b' \in \mathcal{B}$ in time slot t . We have a feasible constraint as follows:

$$\sum_{b' \in \mathcal{B}} \psi_{b,n,t,b'} = 1, \quad \forall b \in \mathcal{B}, n \in \mathbb{N}_{b,t}, t \in \mathcal{T}. \quad (1)$$

3) *Service Delay Model*: AIGC tasks are processed in a first-come-first-served way. That is to say, each task should be processed after the completion of its previous arrival task in the processing queue. Let $T_{b,n,t,b'}^{\text{serv}}$ denote the total service delay of task n that is uploaded to BS b and is offloaded to ES b' for processing in the time slot t . Thus, the $T_{b,n,t,b'}^{\text{serv}}$ includes the task transmission delays from the user end to BS b and from BS b to BS b' , the task computing delay on ES b' , the task waiting time $T_{b,n,t,b'}^{\text{wait}}$ in the processing queue at ES b' , and the transmission delay of generated result from BS b' to BS b and from BS b to the user end. Thus, $T_{b,n,t,b'}^{\text{serv}}$ can be formulated as

$$T_{b,n,t,b'}^{\text{serv}} = \psi_{b,n,t,b'} \cdot \left(\frac{d_n}{v_{n,b',t}} + \frac{\rho_n \cdot z_n}{f_{b'}} + T_{b,n,t,b'}^{\text{wait}} + \frac{\tilde{d}_n}{v_{b',n,t}} \right), \quad (2)$$

where $v_{n,b',t}$ (in bits/s) is the transmission rate from user end to BS b' , $v_{b',n,t}$ (in bits/s) is the transmission rate from BS b' to BS n , $f_{b'}$ (in CPU or GPU cycles/s) is the CPU or GPU computing capacity of ES b' if GPU is available, and \tilde{d}_n is the result (i.e., image) size of processing task n . Thus, $T_{b,n,t,b'}^{\text{wait}}$ can be achieved by

$$T_{b,n,t,b'}^{\text{wait}} = (q_{t-1,b'} + q_{n,t,b'}^{\text{bef}}) / f_{b'}, \quad (3)$$

where $q_{n,t,b'}^{\text{bef}}$ (in CPU or GPU cycles) is the workload length of the processing queue at ES b' before receiving task n , which can be achieved by system observation. $q_{t-1,b'}$ (in CPU or GPU cycles) is the workload length of the processing queue of ES b' at the end of time slot $t-1$, which can be updated by $q_{t,b'} =$

$$\max\{q_{t-1,b'} + \sum_{b \in \mathcal{B}} \sum_{n \in \mathbb{N}_{b,t}} \psi_{b,n,t,b'} \cdot \rho_n \cdot z_n - f_{b'} \Delta, 0\}, \quad (4)$$

where the task workload of each ES at initial time slot 0 is set to 0, i.e., $q_{0,b'} = 0$ for $\forall b' \in \mathcal{B}$, and the queue workload length before task 1 in time slot 0 are set to 0, i.e., $q_{0,0,b'}^{\text{bef}} = 0$ for $\forall b' \in \mathcal{B}$.

B. Problem Formulation

The objective of our problem for efficient AIGC is to minimize the average service delay of all the offloading tasks in the whole system, which is formulated as an online INLP optimization problem:

$$\min_{\psi} \lim_{|\mathcal{T}| \rightarrow \infty} \frac{1}{|\mathcal{T}|} \sum_{t \in \mathcal{T}} \sum_{b \in \mathcal{B}} \sum_{n \in \mathbb{N}_{b,t}} \sum_{b' \in \mathcal{B}} T_{b,n,t,b'}^{\text{serv}} \quad (5)$$

s.t. Eqn. (1),

$$\psi_{b,n,t,b'} \in \{0, 1\}, \quad \forall b, b' \in \mathcal{B}, n \in \mathbb{N}_{b,t}, t \in \mathcal{T}.$$

Here, the optimization variable is task allocation decision $\psi = \{\psi_{b,n,t,b'}\}_{b,b' \in \mathcal{B}, n \in \mathbb{N}_{b,t}, t \in \mathcal{T}}$ in the problem. This offline counterpart of this problem is NP-hard, as proved by the following Theorem 1.

Theorem 1. *The offline counterpart of the problem (5) is an NP-hard problem.*

Proof. The offline counterpart of the problem (5) is proven to be NP-hard through reducing from the multi-knapsack problem [38]. Firstly, all the tasks are viewed as candidate objects in the problem (5). The set \mathcal{B} of ESs is viewed as multi-knapsacks. The tasks offloaded to the ES set are viewed as candidate objects placed into multiple knapsacks under the weight constraints of ES capacities f_1, \dots, f_B . Thus, the problem (5) is a multi-knapsack problem. Secondly, as a general case of the knapsack problem that is well-known NP-hard, the offline counterpart of the problem (5) is also NP-hard. \square

IV. PROPOSED METHOD AND ALGORITHM

This section presents the specific design of our method with the proof of probability derivation and gives our algorithm implementation characterized by linear time complexity.

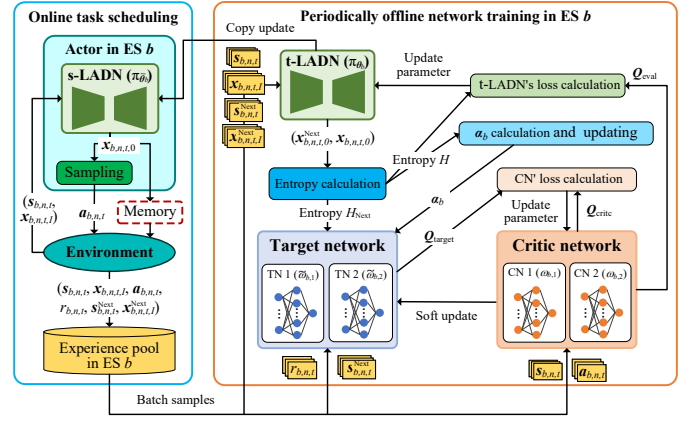


Figure 3. The overall architecture of our method. For each ES b , new arrival AIGC tasks are online offloaded to ESs for parallel processing by the actor. The actor utilizes the system state $s_{b,n,t}$ and historical action probability $\alpha_{b,n,t}$ with edge-edge collaboration. The $\alpha_{b,n,t}$ is stored in memory. The t-LADN model is periodically offline trained using history samples.

A. Method Design

Driven by the NP-hardness of our problem and inspired by the exceptional generation capability of the Denoising Diffusion Probabilistic Model (DDPM) [19], we propose a LAD-TS method to quickly achieve a near-optimal solution to our problem (5) by incorporating the diffusion model and DRL technique. The overall architecture of our LAD-TS method is implemented with the basic SAC [28] framework and reverse diffusion processing as shown in Fig. 3. Our architecture includes two parts: online task scheduling and offline network training. In particular, two Latent Action Diffusion Networks (LADNs), named s-LADN and t-LADN, are designed using reverse diffusion processing. The s-LADN and t-LADNs are used as the two actors in the online task scheduling and the periodic offline training, respectively. In the task scheduling part, the actor will generate a task scheduling decision by the s-LADN according to the inputs of the system state and latent action probability. The network training consists of the t-LADN (the same network structure and parameter as the s-LADN), two Critic Networks (CNs), and two Target Networks (TNs). The t-LADN is periodically trained using the history batch samples extracted from the experience pool. The CNs and TNs have the same network structure, and generate the system's evaluation Q-values Q_{eval} and target Q-values Q_{target} , respectively. Notably, two key improvements of our method are designed: (1) a latent action diffusion strategy to find the near-optimal decision quickly and (2) a periodic offline training mechanism to avoid the poor performance of offline training. The state space, action space, reward function, actor structure, latent action diffusion strategy, and network training will be described as follows.

State space. In our method, each task $n \in \mathbb{N}_{b,t}$ is sequentially processed with one-by-one. Let a vector $s_{b,n,t}$ denote the system state when a task n is arrived at the BS b at time slot t . Intuitively, the arrival task size, the task workload length, and the processing queue length at each ES will affect the decision

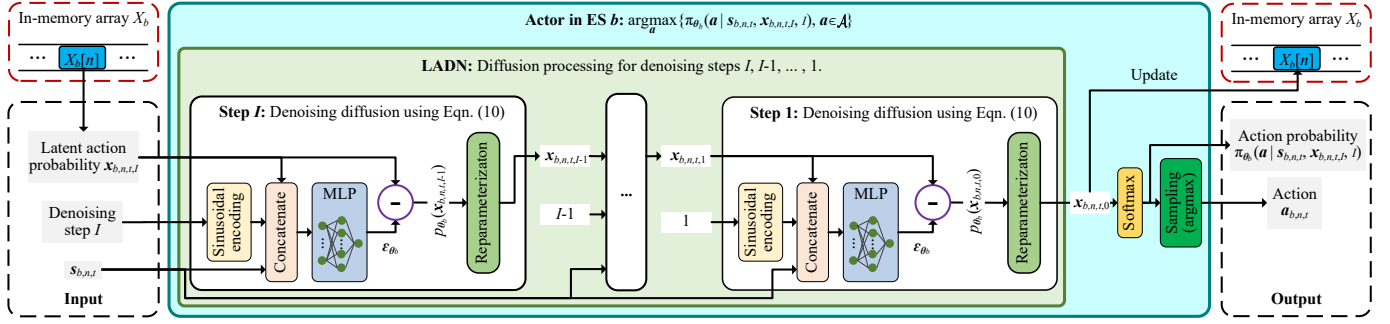


Figure 4. The Actor structure with proposed LADN model. The actor input are the timestep I , latent action probability $\mathbf{x}_{b,n,t,I}$, and system state $\mathbf{s}_{b,n,t}$. The output is the action decision $\mathbf{a}_{b,n,t}$. The historical action probability $\mathbf{x}_{b,n,t,0}$ is stored (or updated) into the array $X_b[n]$.

generation and service delay of task offloading. Thus, $\mathbf{s}_{b,n,t}$ is formulated as

$$\mathbf{s}_{b,n,t} = [d_n, \rho_n \cdot z_n, \mathbf{q}_{t-1}], \quad (6)$$

where $\mathbf{q}_{t-1} = [q_{t-1,1}, q_{t-1,2}, \dots, q_{t-1,B}]$ is achieved by the Eqn. (4). Furthermore, let a variable $\mathbf{s}_{b,n,t}^{\text{next}}$ denote the next system state after offloading a task n . $\mathbf{s}_{b,n,t}^{\text{next}}$ is formulated as

$$\mathbf{s}_{b,n,t}^{\text{next}} = \begin{cases} \mathbf{s}_{b,n+1,t}, & n < N_{b,t}. \\ \mathbf{s}_{b,1,t+1}, & \text{Otherwise.} \end{cases} \quad (7)$$

Action space. We use a binary vector $\mathbf{a}_{b,n,t} = [\psi_{b,n,t,1}, \psi_{b,n,t,2}, \dots, \psi_{b,n,t,B}]$ to represent the action of a task n that is arrived to the BS b at time slot t . Let \mathcal{A} represent the set of all action spaces. We have $\mathcal{A} = \{[1, 0, 0, \dots, 0], [0, 1, 0, \dots, 0], \dots, [0, 0, 0, \dots, 1]\}$. In our problem, an action $\mathbf{a} \in \mathcal{A}$ is determined by our t-LADN, i.e., $\pi_{\theta_b}(\cdot)$, with the inputs of current system state $\mathbf{s}_{b,n,t}$, latent action probability $\mathbf{x}_{b,n,t,I}$, and timestep I . Furthermore, $\mathbf{a}_{b,n,t}$ is formulated as

$$\mathbf{a}_{b,n,t} = \arg \max_{\mathbf{a}} \{\pi_{\theta_b}(\mathbf{a} | \mathbf{s}_{b,n,t}, \mathbf{x}_{b,n,t,I}, I), \forall \mathbf{a} \in \mathcal{A}\}, \quad (8)$$

where $\pi_{\theta_b}(\mathbf{a} | \mathbf{s}_{b,n,t}, \mathbf{x}_{b,n,t,I}, I)$ is the probability of generating the action \mathbf{a} . θ_b is the t-LADN's parameters in ES b .

Reward function. We hope the fewer service delays the more rewards. Thus, the negative task service delay is defined as the reward in our method, i.e., the reward $r_{b,n,t}$ of offloading task n under giving $\mathbf{a}_{b,n,t}$ is formulated as

$$r_{b,n,t} = -T_{b,n,t,b'}^{\text{serv}}. \quad (9)$$

Actor structure. The actor structure consists of a LADN, a softmax unit, and a sampling unit as shown in Fig. 4. The LADN model has I denoising steps. Each denoising step has a sinusoidal encoding unit, a concatenate unit, a Multi-Layer Perception (MLP), and a reparameterization unit. At the first denoising step, the input is the $\mathbf{x}_{b,n,t,I}$, I , and $\mathbf{s}_{b,n,t}$. The output is $\mathbf{x}_{b,n,t,I-1}$. Then, the $\mathbf{x}_{b,n,t,I-1}$, $I-1$, and $\mathbf{s}_{b,n,t}$ are used as the input of the second denoising step. After, followed by the operation of I denoising steps, the action probability $\mathbf{x}_{b,n,t,0}$ will be outputted in the last denoising step. Furthermore, the action probability $\pi_{\theta_b}(\mathbf{a} | \mathbf{s}_{b,n,t}, \mathbf{x}_{b,n,t,I}, I)$ is achieved by taking the softmax operation on $\mathbf{x}_{b,n,t,0}$. Finally,

the optimal $\mathbf{a}_{b,n,t}$ is achieved by the sampling operation using Eqn. (8). Here, the $\mathbf{x}_{b,n,t,0}$ is achieved by the **probability derivation** as shown in the following Theorem 2.

Theorem 2. The action probability $\mathbf{x}_{b,n,t,0}$ is inferred by the update rule: $\mathbf{x}_{b,n,t,i-1} =$

$$\frac{1}{\sqrt{\lambda_i}} (\mathbf{x}_{b,n,t,i} - \frac{\beta_i}{\sqrt{1-\lambda}} \boldsymbol{\epsilon}_{\theta_b}(\mathbf{x}_{b,n,t,i}, i, \mathbf{s}_{b,n,t})) + \frac{\tilde{\beta}_i}{2} \cdot \boldsymbol{\epsilon}, \quad (10)$$

where $i = I, I-1, \dots, 1$, $\beta_i = 1 - e^{-\frac{\beta_{\min}}{I} - \frac{2i-1}{2I^2}(\beta_{\max} - \beta_{\min})}$ represents the forward process variance [19], $\tilde{\beta}_i = \frac{1-\bar{\lambda}_{i-1}}{1-\bar{\lambda}_i} \cdot \beta_i$ is a deterministic variance parameter, $\lambda_i = 1 - \beta_i$, $\bar{\lambda}_i = \prod_{m=1}^i \lambda_m$ is the cumulative production of λ_m over previous m ($m \leq i$) denoising steps, $\lambda_m = 1 - \beta_m$, $\boldsymbol{\epsilon}_{\theta_b}(\mathbf{x}_{b,n,t,i}, i, \mathbf{s}_{b,n,t})$ is the MLP's output, and $\boldsymbol{\epsilon} \sim \mathcal{N}(\mathbf{0}, \mathbf{I})$.

Proof. Firstly, according to the forward diffusion processing in [19], we have

$$\mathbf{x}_{b,n,t,i} = \sqrt{\lambda_i} \cdot \mathbf{x}_{b,n,t,0} + \sqrt{1-\lambda_i} \cdot \boldsymbol{\epsilon}. \quad (11)$$

Secondly, let $p(\mathbf{x}_{b,n,t,i-1} | \mathbf{s}_{b,n,t}, i, \mathbf{x}_{b,n,t,i})$ denote the transition function from $\mathbf{x}_{b,n,t,i}$ to $\mathbf{x}_{b,n,t,i-1}$ and it follows a Gaussian distribution given by $p_{\theta_b}(\mathbf{x}_{b,n,t,i-1} | \mathbf{s}_{b,n,t}, i, \mathbf{x}_{b,n,t,i}) =$

$$\mathcal{N}(\mathbf{x}_{b,n,t,i-1}; \boldsymbol{\mu}_{\theta_b}(\mathbf{x}_{b,n,t,i}, i, \mathbf{s}_{b,n,t}), \tilde{\beta}_i \mathbf{I}), \quad (12)$$

where $i \in \{1, 2, \dots, I\}$, $\boldsymbol{\mu}_{\theta_b}(\mathbf{x}_{b,n,t,i}, i, \mathbf{s}_{b,n,t})$ is the distribution mean and can be learned by a deep model, $\tilde{\beta}_i = \frac{1-\bar{\lambda}_{i-1}}{1-\bar{\lambda}_i} \cdot \beta_i$ is a deterministic variance parameter, $\beta_i = 1 - e^{-\frac{\beta_{\min}}{I} - \frac{2i-1}{2I^2}(\beta_{\max} - \beta_{\min})}$ represents the forward process variance controlled by the variational posterior scheduler [19], $\bar{\lambda}_i = \prod_{m=1}^i \lambda_m$ is the cumulative production of λ_m over previous m ($m \leq i$) denoising steps, and the $\lambda_m = 1 - \beta_m$.

Thirdly, by applying the Bayesian formula and combining the reconstructed sample $\mathbf{x}_{b,n,t,0}$ in Eqn. (11), we have $\boldsymbol{\mu}_{\theta_b}(\mathbf{x}_{b,n,t,i}, i, \mathbf{s}_{b,n,t}) =$

$$\frac{1}{\sqrt{\lambda_i}} (\mathbf{x}_{b,n,t,i} - \frac{\beta_i}{\sqrt{1-\lambda}} \boldsymbol{\epsilon}_{\theta_b}(\mathbf{x}_{b,n,t,i}, i, \mathbf{s}_{b,n,t})). \quad (13)$$

Finally, by employing reparameterization technique for the $p_{\theta_b}(\mathbf{x}_{b,n,t,i-1} | \mathbf{s}_{b,n,t}, i, \mathbf{x}_{b,n,t,i})$, we can get the recurrent relationship as shown in Eqn. (10). \square

Latent Action Diffusion Strategy. Existing diffusion-based DRL methods perform diffusion processing starting from Gaussian noise, which easily leads to divergence in decision-making, degrading their performance. To address this issue, therefore, we design a latent action probability strategy. Specifically, we introduce a latent action probability $\mathbf{x}_{b,n,t,I}$ instead of the random Gaussian noise for each $b \in \mathcal{B}$, $n \in \mathbb{N}_{b,t}$, and $t \in \mathcal{T}$ by considering tasks that usually have a specific periodic pattern over a certain period. For convenience, we assume $N = \max\{N_{b,t}\}_{b \in \mathcal{B}, t \in \mathcal{T}}$ and create an array X_b with length N for each $b \in \mathcal{B}$ to store the historical action probability of task $n \in \mathbb{N}_{b,t}$, where each element $X_b[n]$ is initialized by a standard Gaussian distribution. Then, for each task $n \in \mathbb{N}_{b,t}$ at time slot t , the $\mathbf{x}_{b,n,t,I}$ is achieved by using $X_b[n]$. After executing the diffusion processing, we can get its output $\mathbf{x}_{b,n,t,0}$ and update $X_b[n] \leftarrow \mathbf{x}_{b,n,t,0}$. Furthermore, we also add the $\mathbf{x}_{b,n,t,I}$ to the transition tuple to improve the network training, i.e., using the $(s_{b,n,t}, \mathbf{x}_{b,n,t,I}, \mathbf{a}_{b,n,t}, r_{b,n,t}, s_{b,n,t}^{\text{next}}, \mathbf{x}_{b,n,t,I}^{\text{next}})$ instead of the $(s_{b,n,t}, \mathbf{a}_{b,n,t}, r_{b,n,t}, s_{b,n,t}^{\text{next}})$ in our method. Like this, $\mathbf{x}_{b,n,t,I}$ is further initialized by $\mathbf{x}_{b,n,t-1,0}$. Then, our method can quickly achieve the near-optimal decision by using the historical action probability, which ensures lower service delay than diffusion-based DRL methods.

Network training. To well ensure the effectiveness of diffusion processing, the $\mathbf{x}_{b,n,t}$ is also added to the transition tuple for network training in our method. Let $\tilde{\theta}_b, \omega_{b,1}, \omega_{b,2}, \tilde{\omega}_{b,1}$ and $\tilde{\omega}_{b,2}$ denote the parameters of the s-LADN, CN 1, CN 2, TN 1, and TN 2 in ES b , respectively. Each ES has a trainer to perform network training using batch samples in the experience pool. The parameters of $\theta_b, \tilde{\theta}_b, \{\omega_{b,j}\}_{j=1,2}$, and $\{\tilde{\omega}_{b,j}\}_{j=1,2}$ are updated as follows.

Firstly, K samples are extracted from the experience pool: $\{[s_{b,n,t}^k, \mathbf{x}_{b,n,t}^k, \mathbf{a}_{b,n,t}^k, r_{b,n,t}^k, s_{b,n,t}^{k,\text{next}}, \mathbf{x}_{b,n,t}^{k,\text{next}}]\}_{k=1,2,\dots,K}$. Then, $r_{b,n,t}, s_{b,n,t}^{\text{next}}$, and $\mathbf{x}_{b,n,t}^{\text{next}}$ are inputted to the t-LADN and TNs for Q_{target} calculation. More precisely, $Q_{\text{target}}^k = r_{b,n,t} + \gamma \cdot (\pi_{\theta_b}(a_{b,n,t}^{k,\text{next}} | s_{b,n,t}^{k,\text{next}}, \mathbf{x}_{b,n,t}^{k,\text{next}}, I) \cdot Q_{\text{target}}^{\text{min}} + \alpha_b \cdot H_{\text{next}}^k(\pi_{\theta_b}))$ and $a_{b,n,t}^{k,\text{next}} \sim \pi_{\theta_b}(\cdot | s_{b,n,t}^{k,\text{next}}, \mathbf{x}_{b,n,t}^{k,\text{next}}, I)$, where γ is a reward decay factor and α_b is a temperature coefficient, $Q_{\text{target}}^{\text{min}} = \min_{j=1,2} \{Q_{\tilde{\omega}_{b,j}}(s_{b,n,t}^{k,\text{next}}, a_{b,n,t}^{k,\text{next}})\}$. $H_{\text{next}}^k(\pi_{\theta_b})$ is the entropy of the action probability distribution with the inputs of $s_{b,n,t}^{\text{next}}$ and $\mathbf{x}_{b,n,t}^{\text{next}}$. We have $H_{\text{next}}^k(\pi_{\theta_b}) = -\pi_{\theta_b}(a_{b,n,t}^{k,\text{next}} | s_{b,n,t}^{k,\text{next}}, \mathbf{x}_{b,n,t}^{k,\text{next}}, I)^\top \times \log \pi_{\theta_b}(a_{b,n,t}^{k,\text{next}} | s_{b,n,t}^{k,\text{next}}, \mathbf{x}_{b,n,t}^{k,\text{next}}, I)$.

Secondly, the $\{\omega_{b,j}\}_{j=1,2}$ are updated by minimizing the following critic loss function: $\mathcal{L}_Q(\omega_{b,j}) =$

$$\frac{1}{K} \sum_{k=1}^K (Q_{\omega_{b,j}}(s_{b,n,t}^k, a_{b,n,t}^k) - Q_{\text{target}}^k)^2. \quad (14)$$

Thirdly, the θ_b is updated by minimizing the following actor loss function:

$$\mathcal{L}_\pi(\theta_b) = \frac{1}{K} \sum_{k=1}^K (-\alpha_b \cdot H^k(\pi_{\theta_b}) - \pi_{\theta_b}(a_{b,n,t}^k | s_{b,n,t}^k, \mathbf{x}_{b,n,t}^k, I) \cdot Q_{\text{eval}}^k)^2, \quad (15)$$

where $Q_{\text{eval}}^k = \min_{j=1,2} \{Q_{\omega_{b,j}}(s_{b,n,t}^k, a_{b,n,t}^k)\}$. $H^k(\pi_{\theta_b})$ is the entropy of the action probability

Algorithm 1: Online distributed LAD-TS algorithm

Input: The AIGC task data $\{d_n, z_n\}_{n \in \mathbb{N}_{b,t}, b \in \mathcal{B}, t \in \mathcal{T}}$;
Denosing step I ;

Output: The task allocation decision ψ ;

- 1 Initialize the array X_b by a standard Gaussian distribution for each $b \in \mathcal{B}$;
 - 2 Initialize the LADNs, CNs, and TNs with random $\tilde{\theta}_b, \theta_b, \{\omega_{b,j}\}_{j=1,2}$, and $\{\tilde{\omega}_{b,j}\}_{j=1,2}$ for each $b \in \mathcal{B}$;
 - 3 Initialize the queue $q_{0,b'} = 0$ and the experience pool $\mathcal{R}_{b'} = \emptyset$ for each $b' \in \mathcal{B}$;
 - 4 **for** episode $\in \{1, 2, \dots, E\}$ **do**
 - 5 Reset system environment;
 - 6 **foreach** time slot $t \in \mathcal{T}$ **do**
 - 7 **for** all BS $b \in \mathcal{B}$ in parallel **do**
 - 8 **foreach** new arrival task $n \in \mathbb{N}_{b,t}$ **do**
 - 9 Observe $s_{b,n,t}$ and $\mathbf{x}_{b,n,t,I} \leftarrow X_b[n]$;
 - 10 Generate $\mathbf{x}_{b,n,t,0}$ and $\mathbf{a}_{b,n,t}$ by the Actor model;
 - 11 Calculate $r_{b,n,t}$ using Eqn. (9);
 - 12 Update $X_b[n] \leftarrow \mathbf{x}_{b,n,t,0}$;
 - 13 Observe $s_{b,n,t}^{\text{next}}$ and $\mathbf{x}_{b,n,t,I}^{\text{next}}$;
 - 14 Store the tuple $(s_{b,n,t}, \mathbf{x}_{b,n,t,I}, \mathbf{a}_{b,n,t}, r_{b,n,t}, s_{b,n,t}^{\text{next}}, \mathbf{x}_{b,n,t,I}^{\text{next}})$ to \mathcal{R}_b ;
 - 15 **if** $|\mathcal{R}_b| > 300$ **then**
 - 16 Sample K tuples from \mathcal{R}_b ;
 - 17 Execute network training to update $\{\omega_{b,j}\}_{j=1,2}, \theta_b, \alpha_b$, and $\{\tilde{\omega}_{b,j}\}_{j=1,2}$ using Eqns. (14) - (17);
 - 18 Update $\tilde{\theta}_b$ by copying θ_b ;
 - 19 Update q_t by the Eqn. (4);
-

distribution with the inputs of $s_{b,n,t}$ and $\mathbf{x}_{b,n,t}$. We have $H^k(\pi_{\theta_b}) = -\pi_{\theta_b}(a_{b,n,t}^k | s_{b,n,t}^k, \mathbf{x}_{b,n,t}^k, I)^\top \times \log \pi_{\theta_b}(a_{b,n,t}^k | s_{b,n,t}^k, \mathbf{x}_{b,n,t}^k, I)$.

Fourthly, the α_b is updated by minimizing the entropy loss function for each BS $b \in \mathcal{B}$:

$$\mathcal{L}(\alpha_b) = (-H^k(\pi_{\theta_b}) - \tilde{H}) \cdot \alpha_b, \quad (16)$$

where \tilde{H} is a hyper-parameter of target entropy.

Finally, the $\{\tilde{\omega}_{b,j}\}_{j=1,2}$ are updated by the soft updating operation as:

$$\tilde{\omega}_{b,j} = \tau_b \cdot \omega_{b,j} + (1 - \tau_b) \cdot \tilde{\omega}_{b,j}, \quad (17)$$

where the τ_b is the weight of the soft updating operation. The $\tilde{\theta}_b$ is updated by copying θ_b .

B. Algorithm Implementation

We implement our LAD-TS method as an online distributed algorithm, as shown in Algorithm 1. In this algorithm, the inputs are the AIGC tasks with their data $\{d_n, z_n\}_{n \in \mathbb{N}_{b,t}}$ and denoising step I . The output is the task allocation decision ψ . The Algorithm 1 works as follows.

Step 1. It begins by initializing each element $X_b[n]$ in the array X_b with a standard Gaussian distribution for each task $n \in \mathbb{N}_{b,t}$ and $b \in \mathcal{B}$ (Line 1). Then, for each BS $b \in \mathcal{B}$, LADNs, CNs, and TNs are initialized with random parameters $\tilde{\theta}_b$, θ_b , $\{\omega_{b,j}\}_{j=1,2}$, and $\{\tilde{\omega}_{b,j}\}_{j=1,2}$, respectively (Line 2). The queue $q_{0,b'}$ and the experience pool $\mathcal{R}_{b'}$ at each BS $b' \in \mathcal{B}$ are initialized to 0 and empty \emptyset , respectively (Line 3).

Step 2. For each episode $= 1, 2, \dots, E$, the system environment is reset. Then, for each time slot $t \in \mathcal{T}$ and each task $n \in \mathbb{N}_{b,t}$ in a parallel way (Lines 6 - 8), the system state $s_{b,n,t}$ and latent action probability $x_{b,n,t,I}$ are observed from the environment and X_b , respectively (Line 9). Then, by utilizing the $s_{b,n,t}$ and $x_{b,n,t,I}$, and I as input, the action $a_{b,n,t}$ and $x_{b,n,t,0}$ are generated by the Actor (Line 10). Accordingly, the reward $r_{b,n,t}$ is calculated using Eqn. (9) (Line 11). Furthermore, the $x_{b,n,t,I}$ is updated by equating to $x_{b,n,t,0}$ (Line 12). The next system state $s_{b,n,t}^{\text{next}}$ and latent action probability $x_{b,n,t,I}^{\text{next}}$ are observed from the environment and X_b , respectively (Line 13). The transition tuple $(s_{b,n,t}, x_{b,n,t,I}, a_{b,n,t}, r_{b,n,t}, s_{b,n,t}^{\text{next}}, x_{b,n,t,I}^{\text{next}})$ is stored to the experience pool \mathcal{R}_b (Line 14).

Step 3. If the size $|\mathcal{R}_b|$ of experience pool exceeds 300, K samples from \mathcal{R}_b are extracted to sequentially update the model parameters $\{\omega_{b,j}\}_{j=1,2}$, θ_b , α_b , and $\{\tilde{\omega}_{b,j}\}_{j=1,2}$ (Lines 15 - 17). After the completion of network training, the parameter $\tilde{\theta}_b$ is updated by copying θ_b (Line 18). Here, $|\mathcal{R}_b| > 300$ is set to control that at least 300 history tuples have been stored, ensuring model training based on user-defined real-world conditions [28].

Step 4. At the end of each time slot, the queue q_t is updated according to the Eqn. (4) (Line 19).

Finally, the near-optimal task allocation policy $\pi_{\tilde{\theta}}$ is gradually learned through the above steps. Here, for each time slot t , the time complexity of Algorithm 1 is a linear time complexity $O(N_{b,t})$ as proved in the following Theorem 3.

Theorem 3. For each time slot t , the time complexity of Algorithm 1 is a linear time complexity $O(N_{b,t})$.

Proof. As shown in Algorithm 1, for each time slot $t \in \mathcal{T}$, there are two “for” loops orderly. In the first loop, since all BSs are executed in parallel, its time complexity is $O(1)$. In the second loop, the time complexity is determined by the number of tasks $N_{b,t}$, the solving time of ES selection, and the network training time. Furthermore, the time complexity of ES selection is $O(1)$ since the t-LADN model has been trained previously. Meanwhile, the network training is performed offline. Thus, the total time complexity of Algorithm 1 is $O(N_{b,t})$ for each time slot t . \square

V. PERFORMANCE EVALUATION

In this section, we develop a simulator in Python to evaluate the effectiveness of our method with insightful analysis.

A. Setup

Environment Parameters. The number of BSs (B) is set to 20 [25]. The number of tasks arriving at each BS during

Table III
DEFAULT SETTING OF ENVIRONMENT PARAMETER.

Param.	Value	Param.	Value
B	20 [25]	$ \mathcal{T} $	60 [39]
$N_{b,t}$	[1, 50] [39]	Δ	1.0 second [30]
ρ_n	[100, 300] cycles/bit [15]	d_n	[2, 5] Mbits [39]
$v_{b,b',t}$	[400, 500] Mbits/s [15]	$f_{b'}$	[10, 50] GHz [15]

Table IV
DEFAULT SETTING OF MODEL PARAMETERS.

Parameters	Value
Hidden layers of actor and CN	2 full connection (20, 20)
Learning rate η_a	1e-4
Learning rate η_c	1e-3
Learning rate η_α	3e-4
Reward decay's factor γ	0.95
Soft updating's weight τ	0.005
Batch size K	64
Denosing step I	5
Entropy temperature α	0.05
Target entropy \tilde{H}	-1
Number of episodes E	60
Experience pool's size $ \mathcal{R} $	1000
Optimizer	Adam

time slot t ($N_{b,t}$) is randomly generated within the range [1, 50] [39]. The total number of time slots $|\mathcal{T}|$ is 60, corresponding to a duration of 1 minute, with each time slot t lasting 1 second. Task sizes d_n are randomly chosen between [2, 5] Mbits [39], while the size \tilde{d}_n of the generated images is set between [0.6, 1.0] Mbits, equivalent to a resolution of 512×512 pixels. The required image generation quality z_n and computation resources ρ_n are set within the ranges of [1, 15] steps [25] and [100, 300] CPU cycles/step, respectively. The computational capacity of each ES, $f_{b'}$, ranges from [10, 50] GHz [15]. The data transmission rates $v_{n,b',t}$ and $v_{b',n,t}$ are uniformly distributed between [400, 500] Mbits/s [15].

Model Parameters. We construct the DRL model using the PyTorch framework. The LADNs, CNs, and TNs are all configured as an MLP, each comprising one input layer, two hidden layers with 20 neurons each, and one output layer. Consistent with the findings in [25], we set the reward decay factor γ to 0.95. The experience replay buffer \mathcal{R}_b at each ES has a capacity of 1000. The learning rates for the LADNs, CNs, and α_b are $1e-4$, $1e-3$, and $3e-4$, respectively. We use a batch size of 64 and the Adam optimizer. The initial value of α_b is 0.05, and the target entropy \tilde{H} is -1.0 . Lastly, the weight coefficient τ_b is set to 0.005 and the denosing step I is set to 5 according to our experiments as shown in Fig. 8.

B. Baselines

We use two well-established DRL baselines, a diffusion-based DRL baseline, and a heuristic optimal baseline to compare performance with our method as follows.

DQN-TS. The DQN [27] is a well-known DRL method that has been widely applied to various fields. In our experiments,

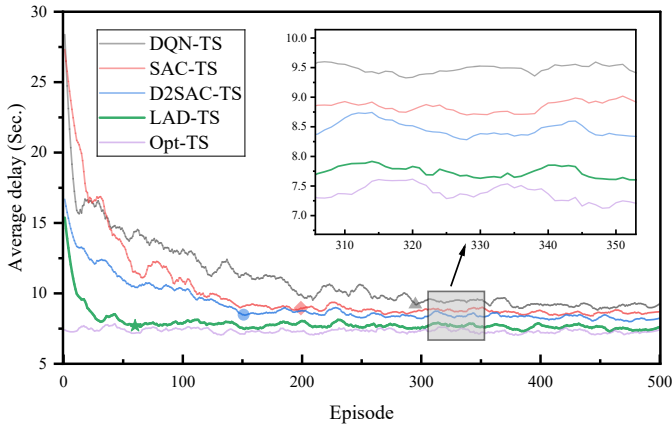


Figure 5. The average service delays of our LAD-TS method and baselines with increasing training episodes.

we faithfully implement the DQN-based Task Scheduling (DQN-TS) method as a baseline with the same setup.

SAC-TS. The SAC [28] is the state-of-the-art DRL-based method. We further implement the SAC-based Task Scheduling (SAC-TS) method as another baseline with the same setup.

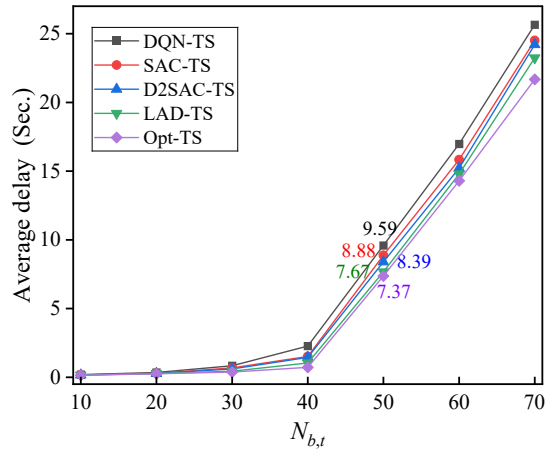
D2SAC-TS [25]. We use the D2SAC-TS as the baseline which is the state-of-the-art task scheduling method based on the diffusion model and DRL.

Opt-TS. An optimal method selects the most suitable ES to process each task by enumerating all action spaces. Opt-TS provides the upper bound on the performance of AIGC services, but it is infeasible since the scheduler has no way of knowing in advance the compute and network resources available for ESs in the actual edge system.

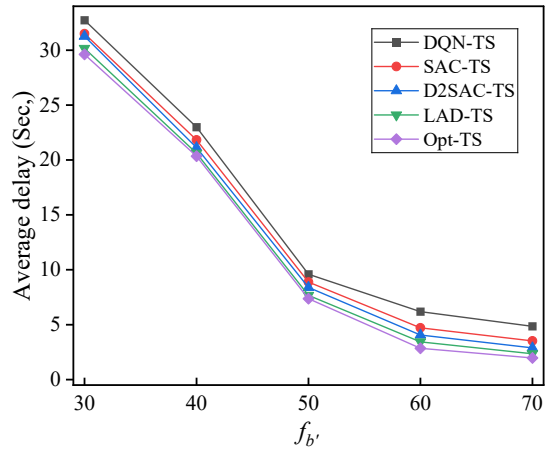
C. Results

We first assess the learning performance of our method against four baselines, as depicted in Fig. 5. The x -axis represents the episode count, while the y -axis indicates each episode’s average service delay across tasks and time slots. Subsequently, we compare the average service delay of our method with the baselines by varying environment parameters as illustrated in Figs. 6 and 7, and analyze the model parameters of denoising step and entropy temperature impact on the service delay of our method as shown in Fig. 8. We perform 50 independent experiments to achieve these results.

Learning Performance Evaluation. To gain insights into the learning performance of our LAD-TS method, we compare its performance with the baselines, as illustrated in Fig. 5. With increasing training episodes, this figure shows that our LAD-TS method’s delay initially decreases and then reaches convergence after only **60** training episodes. In contrast, the delays for the DQN-TS, SAC-TS, and D2SAC-TS methods require 300, 200, and 150 training episodes to converge, respectively. Consequently, the LAD-TS method reduces the number of training episodes by **80%** for DQN-TS, **70%** for SAC-TS, and **60%** for D2SAC-TS. This efficiency is attributed to the LAD-TS method’s capability to make multi-step diffusion decisions



(a) Varying the number of tasks.

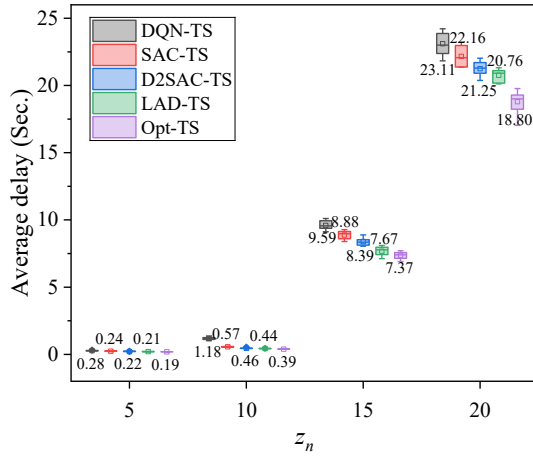


(b) Varying the ESs’ capacities.

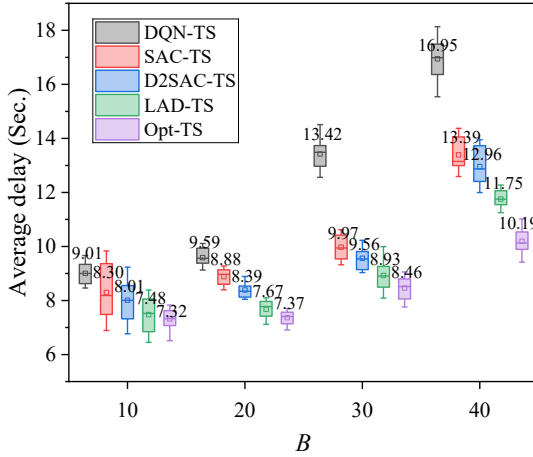
Figure 6. The comparison results of our method and baselines by varying the number of tasks and the ESs’ capacities.

with historical action probability guidance instead of Gaussian noise, accelerating the convergence process. On the other hand, from the subfigure in Fig. 5, the average service delays for the DQN-TS, SAC-TS, D2SAC-TS, and LAD-TS methods stabilize at about 9.5, 8.9, 8.4, and **7.7** seconds, respectively. These results show that our LAD-TS method achieves the lowest delay and significantly outperforms the delays of DQN-TS, SAC-TS, and D2SAC-TS methods. Notably, our LAD-TS method closely approximates the heuristic optimal method’s (Opt-TS) delay of 7.4 seconds. This trend is observed because our LAD-TS method progressively improves policy learning by utilizing the diffusion model’s condition generation capability and the DRL’s environment interaction ability, thereby approaching an optimal policy.

Performance Comparison. Figs. 6 and 7 present the average service delay comparison between our LAD-TS method and four baseline approaches. Specifically, Fig. 6(a) demonstrates how the service delays for all four methods escalate as the upper bound $N_{b,t}$ —representing the number of tasks arriving at each BS—increases from 10 to 70. This escalation



(a) Varying the AIGC qualities.



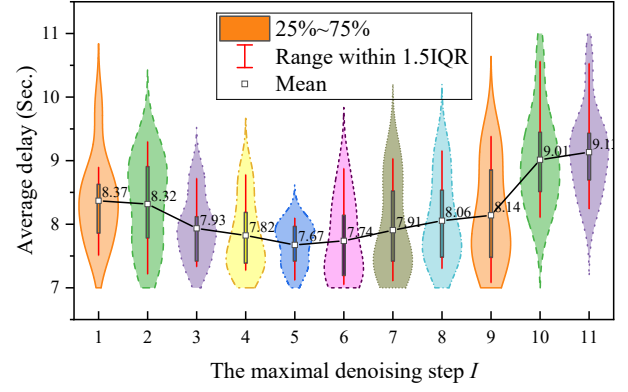
(b) Varying the number of BSs.

Figure 7. The comparison results of our method and baselines by varying the AIGC qualities and the number of BSs.

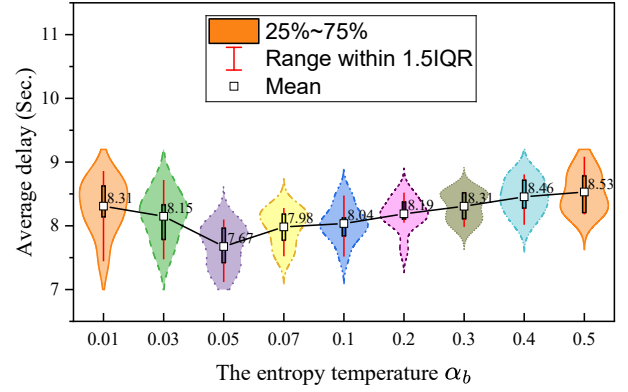
is intuitive, i.e., a higher number of tasks leads to an increased workload being offloaded to the ESs, thereby elevating the service delay. Nonetheless, our LAD-TS method consistently exhibits lower service delays than the DQN-TS, SAC-TS, and D2SAC-TS methods, mirroring the optimal results as $N_{b,t}$ increases from 10 to 70. For instance, when $N_{b,t}$ equals 50, the average service delay of our LAD-TS method is only **7.67** seconds which is significantly lower than those (**9.59**, **8.88**, and **8.39** seconds) of the DQN-TS, SAC-TS, and D2SAC-TS methods by **20.02%**, **13.63%**, and **8.58%**, respectively. Also, this result is close to the Opt-TS method's service delay of 7.37 seconds.

Furthermore, we explore the impact of varying the upper bound $f_{b'}$ of ESs' capacities on service delay, as depicted in Fig. 6(b). From Fig. 6(b), we can see that the average service delays for all methods decrease with increasing $f_{b'}$ within the range [30, 70]. However, our LAD-TS method consistently outperforms the DQN-TS, SAC-TS, and D2SAC-TS methods across the $f_{b'}$ variations.

The results presented in Fig. 7(a) are achieved by varying



(a) Our method's denoising step impact on service delay.



(b) Our method's entropy temperature impact on service delay.

Figure 8. The service delay of our method by varying denoising step I and entropy temperature α_b .

the quality demand z_n of image generation. Echoing the trends observed in Fig. 6(a), as z_n increases from 5 to 20, our LAD-TS method consistently surpasses the DQN-TS, SAC-TS, and D2SAC-TS methods in minimizing service delay, closely aligning with the optimal results. Notably, at a z_n value of 20, the average service delay for our LAD-TS method is recorded at 18.80 seconds. In contrast, the average service delays for the DQN-TS, SAC-TS, and D2SAC-TS methods are recorded at 23.11, 21.25, and 20.76 seconds, respectively, which are higher than that of our LAD-TS method by 22.92%, 13.03%, and 10.42% respectively.

Besides, we also test the impact of varying the number B of BSs on service delay, as illustrated in Fig. 7(b). Fig. 7(b) reveals that service delays escalate for all methods as B increases. Nonetheless, our LAD-TS method consistently outperforms the DQN-TS, SAC-TS, and D2SAC-TS methods across these variations. Moreover, as B grows, the relative delay advantage of LAD-TS becomes more pronounced. When B is set to 40, the LAD-TS method achieves an average service delay of 11.75 seconds which reduces the service delays (16.95, 13.39, and 12.96 seconds) of the DQN-TS, SAC-TS, and D2SAC-TS methods by **30.67%**, **12.25%**, and **9.34%**, respectively. This superior performance is due to the LAD-TS method's ability to leverage the guidance from latent actions,

which effectively optimizes the action policy to accommodate an increasing number of BSs with incoming tasks.

These findings prove that our LAD-TS method significantly outperforms existing state-of-the-art methods in reducing the service delay between **8.58%** to **30.67%** while closely approximating optimal outcomes.

Key Parameter Analysis. Two key parameters of denoising step I and entropy temperature α_b are introduced to ensure computational efficiency and performance in our LAD-TS method. Specifically, setting the appropriate values for I and α_b involves a trade-off between computational efficiency and performance. Fig. 8(a) presents the service delay of our method as the denoising step increases. Generally, a large value of I is recommended to ensure image generation quality in the SD model, but this also leads to longer computation times [19]. However, from Fig. 8(a), we can see that when I equals 5, our LAD-TS method achieves the lowest service delay and maintains a small error distribution.

In DRL, the action entropy regularization term is introduced to balance exploration and exploitation [28], with its behavior controlled by the entropy temperature value α_b . To assess its impact on the performance of our LAD-TS method, we evaluate the average service delay by varying the entropy temperature α_b , as shown in Fig. 8(b). The results reveal that as α_b increases from 0.01 to 0.5, the average service delay first decreases and then begins to rise. The optimal value for minimizing service delay is found to be $\alpha = 0.05$, which strikes a balance between exploration and exploitation. Specifically, lower values of α_b lead to overly greedy behavior, restricting the agent from exploring actions with higher uncertainty, which can prevent the discovery of more effective actions. On the other hand, higher values of α encourage excessive randomness, potentially hindering the agent’s ability to converge on an optimal policy efficiently.

The above findings suggest that the moderate values of $\alpha = 0.05$ and $I = 5$ facilitate faster convergence and better performance by promoting effective exploration-exploitation and computational-performance trade-offs. This balance is crucial for ensuring the efficiency and optimality of the task scheduling policy learned by our LAD-TS method.

VI. IMPLEMENTATION AND VALIDATION

In this section, we develop a prototype system to implement our DEdgeAI as shown in Fig. 9. The practicality of our LAD-TS method is further validated in the prototype system. The test-results are presented in Table V and Fig. 11.

A. System Implementation and Algorithm Deployment

As depicted in Fig. 9, our DEdgeAI system is implemented on five Jetson AGX Orin devices. Each device is equipped with the NVIDIA Ampere architecture GPU, featuring 2048 CUDA cores and 64 Tensor Cores. These devices serve as the ESs in our DEdgeAI system. The scheduler integrated with our Algorithm 1 is also deployed on each Jetson. The devices are interconnected through a wired Gigabit local area

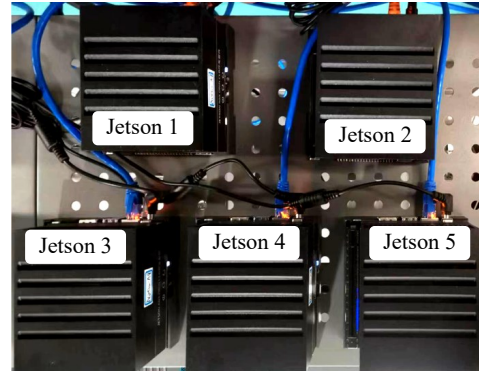


Figure 9. DEdgeAI is implemented on five Jetsons.

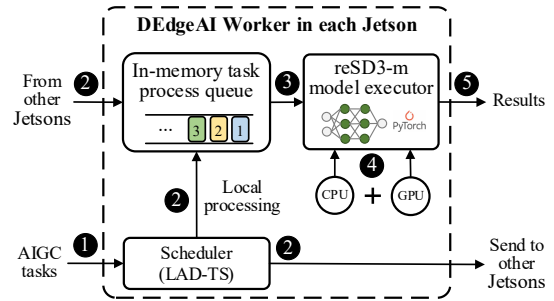


Figure 10. An instance of DEdgeAI worker in each Jetson.

network, enabling the DEdgeAI system to process incoming AIGC requests collaboratively in a distributed manner.

We select the text-to-image task as a representative example to validate our LAD-TS method in the DEdgeAI system. Specifically, we first observe that the original SD3 medium model has 8 billion parameters [40]. Moreover, it uses three pretrained text encoders— OpenCLIP-ViT/G, CLIP-ViT/L, and T5xxl—to encode text representations, and an improved autoencoding model to encode image tokens, which require large memory and leads to a low inference efficiency for edge devices. To address these issues, we then implement the reSD3-m model by removing the T5xxl encoder of the original SD3 medium model [22]. Finally, we deploy the reSD3-m model into each Jetson for providing text-to-image services.

B. Experimental Design

Dataset. We utilize the publicly available Flickr8k dataset. In particular, the text labels of the Flickr8k dataset are extracted as the input of AIGC tasks.

DEdgeAI Worker. As shown in Fig. 10, for each Jetson device b at time slot t , we randomly select $N_{b,t}$ text labels from the dataset to prompt AIGC tasks (1). The scheduler on each Jetson device then employs our LAD-TS algorithm to offload these tasks so they can be processed successfully (2, 3, and 4). Finally, the results are achieved (5). The variables d_n and \tilde{d}_n represent the actual lengths of the task’s input (a text or an image) and the processed output (an image), respectively. We calculate the service delay as the elapsed time from initiating task transmission to receiving the processed result.

Table V

THE EXPERIMENTAL RESULTS OF THE TOTAL GENERATION DELAY OF OUR DEDGEAI SYSTEM AND EXISTING REPRESENTATIVE PLATFORMS UNDER DIFFERENT NUMBERS OF AIGC TASKS.

Platform or system	Model	Median generated delay (Sec.)				Price per 1K images (USD)
		$ \mathcal{N} =1$	$ \mathcal{N} =100$	$ \mathcal{N} =500$	$ \mathcal{N} =1000$	
Midjourney	Midjourney v6	75.9	7590.0	37950.0	75900.0	\$66.00
OpenAI	DALL-E3	14.7	1470.0	7350.0	14700.0	\$40.00
Replicate	SD1.5	32.9	3290.0	16450.0	32900.0	\$8.56
Deepinfra	SD2.1	12.7	1270.0	6350.0	12700.0	\$3.76
Stability.AI	SD3	5.4	540.0	2700.0	5400.0	\$65.00
DEdgeAI (Ours)	reSD3-m	18.3	382.4	1921.5	3895.4	Free

* Note that the data of Midjourney [4], OpenAI [18], Replicate [41], Deepinfra [42], and Stability.AI [43] platforms are achieved from <https://artificialanalysis.ai/text-to-image>.

C. Test-bed Results

We compare the total generation delay of our DEdgeAI system with that of existing state-of-the-art platforms across varying task counts, as detailed in Table V. The results indicate that for a single task, DEdgeAI exhibits a higher image generation delay than OpenAI, Deepinfra, and Stability.AI, due to the comparatively lower AI performance of the edge Jetson device used in our DEdgeAI. However, our DEdgeAI outperforms Midjourney and Replicate even with a single task. Notably, as the number of AIGC tasks increases to greater than 100, DEdgeAI always achieves the lowest image generation delay relative to all five platforms. Moreover, when the number of AIGC tasks equals 100, DEdgeAI reduces the service delays by **94.96%**, **73.98%**, **88.37%**, **69.89%**, and **29.18%** compared to Midjourney, OpenAI, Replicate, Deepinfra, and Stability.AI, respectively. This is because both LAD-TS and parallel processing are designed in our DEdgeAI system, significantly reducing service delays for large task requests. Additionally, the Midjourney, OpenAI, Replicate, Deepinfra, and Stability.AI platforms incur costs of \$66.00, \$40.00, \$8.56, \$3.76, and \$65.00 for generating 1000 images, respectively, but our DEdgeAI offers a generation-free solution as it can be self-developed and deployed.

We test the memory occupations of the reSD3-m model and the original SD3 medium model in our DEdgeAI system. Experimental results show that using the original SD3 medium model occupies about 40 GB memory. However, when the reSD3-m model is used, the DEdgeAI memory is only occupied by about **16 GB**, reducing the memory using by **60%** compared to the original SD3 medium model.

We also examine the image generation quality of our DEdgeAI system, with selective results depicted in Fig. 11. Although these results have a lower quality compared to the SD3 model, they satisfactorily meet the task requirements, further confirming the practical applicability of our LAD-TS method in real-world edge systems. However, the image

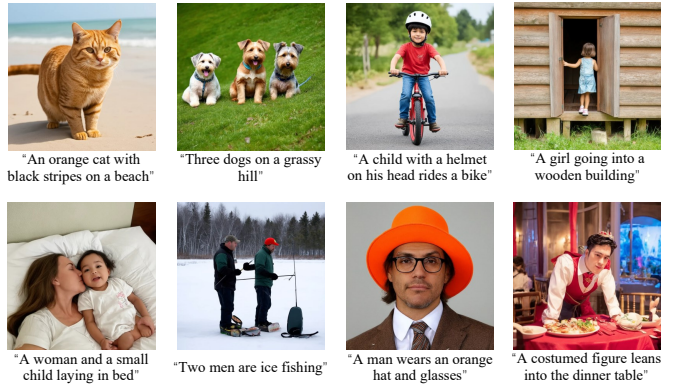


Figure 11. The partial experimental results for AIGC tasks by our DEdgeAI system. Intuitively, these results match the requirements of the task well. Importantly, the total image generation delay of our DEdgeAI system is significantly lower than that of existing platforms as shown in Table V.

generation quality is beyond the primary scope of this study.

D. Scalability Discussion

Our LAD-TS method presents the integration of the diffusion model and the SAC framework, improving task scheduling policy. However, the LAD-TS could be incorporated into other DRL methods, e.g., DQN. Additionally, although our DEdgeAI system demonstrates a text-to-image application in the test-bed results, it also can adapt to many contemporary applications, such as text-to-text and text-to-video. These analyses led us to design a general latent action diffusion paradigm for DRL and extend our DEdgeAI to more AIGC applications in future work.

VII. CONCLUSION

In this paper, we address the distributed AIGC challenge within collaborative edge environments by formulating it as an online ILP problem focused on minimizing task service delays for a real AIGC service. We propose a novel LAD-TS method for task scheduling by incorporating the diffusion model and DRL technique. Moreover, we design a latent action diffusion strategy to optimize task scheduling policy with the proof of probability derivation, improving the AIGC QoE and training time. We implement the LAD-TS as an online distributed algorithm that is characterized by linear time complexity. Furthermore, we develop the DEdgeAI system with our LAD-TS method and implement a refined AIGC service deployment. Extensive simulations underscore our method's superiority, achieving service delay reductions between 8.58% and 30.67% while closely approximating optimal outcomes. Also, LAD-TS significantly decreases the required training episodes by at least 60%. Empirical tests on the DEdgeAI system reveal at least a 29.18% improvement in service delay and a 60% reduction in memory occupation over existing representative AIGC platforms. This research represents a meaningful advancement in distributed edge systems for AIGC services.

REFERENCES

- [1] Y. Cao, S. Li, Y. Liu, Z. Yan, Y. Dai, P. S. Yu, and L. Sun, "A comprehensive survey of ai-generated content (aigc): A history of generative ai from gan to chatgpt," *arXiv preprint arXiv:2303.04226*, pp. 1–44, 2023.
- [2] S. Wang, Z. Shao, and J. C. Lui, "Next-word prediction: A perspective of energy-aware distributed inference," *IEEE Transactions on Mobile Computing*, vol. 23, no. 5, pp. 5695–5708, 2024.
- [3] L. Ouyang, J. Wu, X. Jiang, D. Almeida, C. Wainwright, P. Mishkin, C. Zhang, S. Agarwal, K. Slama, A. Ray *et al.*, "Training language models to follow instructions with human feedback," *Advances in Neural Information Processing Systems*, vol. 35, pp. 27 730–27 744, 2022.
- [4] Midjourney Platform: <https://www.midjourney.com/home>.
- [5] Y. Liu, K. Zhang, Y. Li, Z. Yan, C. Gao, R. Chen, Z. Yuan, Y. Huang, H. Sun, J. Gao *et al.*, "Sora: A review on background, technology, limitations, and opportunities of large vision models," *arXiv preprint arXiv:2402.17177*, 2024.
- [6] Y. Lin, Z. Gao, H. Du, D. Niyato, J. Kang, Z. Xiong, and Z. Zheng, "Blockchain-based efficient and trustworthy aigc services in metaverse," *IEEE Transactions on Services Computing*, 2024.
- [7] Hugging Face Platform: <https://huggingface.co/spaces>.
- [8] R. Zhang, R. Zhou, Y. Wang, H. Tan, and K. He, "Incentive mechanisms for online task offloading with privacy-preserving in uav-assisted mobile edge computing," *IEEE/ACM Transactions on Networking*, 2024.
- [9] S. Ye, L. Zeng, X. Chu, G. Xing, and X. Chen, "Asteroid: Resource-efficient hybrid pipeline parallelism for collaborative dnn training on heterogeneous edge devices," in *Proceedings of the 30th Annual International Conference on Mobile Computing and Networking*, 2024, pp. 312–326.
- [10] B. Wang, D. Irwin, P. Shenoy, and D. Towsley, "Invar: Inversion aware resource provisioning and workload scheduling for edge computing," in *IEEE INFOCOM 2024-IEEE Conference on Computer Communications*. IEEE, 2024, pp. 1–10.
- [11] R. Li, T. Ouyang, L. Zeng, G. Liao, Z. Zhou, and X. Chen, "Online optimization of dnn inference network utility in collaborative edge computing," *IEEE/ACM Transactions on Networking*, 2024.
- [12] R. Han, S. Wen, C. H. Liu, Y. Yuan, G. Wang, and L. Y. Chen, "Edgetuner: Fast scheduling algorithm tuning for dynamic edge-cloud workloads and resources," in *IEEE INFOCOM 2022-IEEE Conference on Computer Communications*. IEEE, 2022, pp. 880–889.
- [13] T. Wang, Y. Liang, X. Shen, X. Zheng, A. Mahmood, and Q. Z. Sheng, "Edge computing and sensor-cloud: Overview, solutions, and directions," *ACM Computing Surveys*, vol. 55, no. 13, pp. 1–37, 2023.
- [14] C. Xu, J. Guo, Y. Li, H. Zou, W. Jia, and T. Wang, "Dynamic parallel multi-server selection and allocation in collaborative edge computing," *IEEE Transactions on Mobile Computing*, pp. 1–15, 2024.
- [15] W. Fan, L. Zhao, X. Liu, Y. Su, S. Li, F. Wu, and Y. Liu, "Collaborative service placement, task scheduling, and resource allocation for task offloading with edge-cloud cooperation," *IEEE Transactions on Mobile Computing*, vol. 23, no. 1, pp. 238–256, 2024.
- [16] L. He, G. Sun, Z. Sun, P. Wang, J. Li, S. Liang, and D. Niyato, "An online joint optimization approach for qoe maximization in uav-enabled mobile edge computing," in *IEEE INFOCOM 2024-IEEE Conference on Computer Communications*. IEEE, 2024, pp. 1–10.
- [17] A. Khochare, F. B. Sorbelli, Y. Simmhan, and S. K. Das, "Improved algorithms for co-scheduling of edge analytics and routes for uav fleet missions," *IEEE/ACM Transactions on Networking*, vol. 32, no. 1, pp. 17–33, 2023.
- [18] DALL-E Platform: <https://openai.com/index/dall-e/>.
- [19] J. Ho, A. Jain, and P. Abbeel, "Denosing diffusion probabilistic models," *Advances in neural information processing systems*, vol. 33, pp. 6840–6851, 2020.
- [20] H. Du, J. Wang, D. Niyato, J. Kang, Z. Xiong, and D. I. Kim, "Ai-generated incentive mechanism and full-duplex semantic communications for information sharing," *IEEE Journal on Selected Areas in Communications*, 2023.
- [21] E. A. Van Dis, J. Bollen, W. Zuidema, R. Van Rooij, and C. L. Bocking, "Chatgpt: five priorities for research," *Nature*, vol. 614, no. 7947, pp. 224–226, 2023.
- [22] Stable Diffusion 3-Medium: <https://github.com/Stability-AI/sd3-ref/tree/master>.
- [23] M. Maaz, H. Rasheed, S. Khan, and F. S. Khan, "Video-chatgpt: Towards detailed video understanding via large vision and language models," *arXiv preprint arXiv:2306.05424*, 2023.
- [24] C. Xu, J. Guo, J. Zeng, S. Meng, X. Chu, J. Cao, and T. Wang, "Enhancing ai-generated content efficiency through adaptive multi-edge collaboration," in *2024 IEEE 44th International Conference on Distributed Computing Systems (ICDCS)*. IEEE, 2024, pp. 960–970.
- [25] H. Du, Z. Li, D. Niyato, J. Kang, Z. Xiong, H. Huang, and S. Mao, "Diffusion-based reinforcement learning for edge-enabled ai-generated content services," *IEEE Transactions on Mobile Computing*, 2024.
- [26] M. Xu, D. Niyato, H. Zhang, J. Kang, Z. Xiong, S. Mao, and Z. Han, "Sparks of generative pretrained transformers in edge intelligence for the metaverse: Caching and inference for mobile artificial intelligence-generated content services," *IEEE Vehicular Technology Magazine*, vol. 18, no. 4, pp. 35–44, 2023.
- [27] V. Mnih, K. Kavukcuoglu, D. Silver, A. A. Rusu, J. Veness, M. G. Bellemare, A. Graves, M. Riedmiller, A. K. Fidjeland, G. Ostrovski *et al.*, "Human-level control through deep reinforcement learning," *nature*, vol. 518, no. 7540, pp. 529–533, 2015.
- [28] T. Haarnoja, A. Zhou, P. Abbeel, and S. Levine, "Soft actor-critic: Off-policy maximum entropy deep reinforcement learning with a stochastic actor," in *Proceedings of the 35th International Conference on Machine Learning (PMLR)*, vol. 80. PMLR, 2018, pp. 1861–1870.
- [29] Z. Tang, F. Mou, J. Lou, W. Jia, Y. Wu, and W. Zhao, "Multi-user layer-aware online container migration in edge-assisted vehicular networks," *IEEE/ACM Transactions on Networking*, 2023.
- [30] M. Tang and V. W. Wong, "Deep reinforcement learning for task offloading in mobile edge computing systems," *IEEE Transactions on Mobile Computing*, vol. 21, no. 6, pp. 1985–1997, 2022.
- [31] N. C. Luong, D. T. Hoang, S. Gong, D. Niyato, P. Wang, Y.-C. Liang, and D. I. Kim, "Applications of deep reinforcement learning in communications and networking: A survey," *IEEE communications surveys & tutorials*, vol. 21, no. 4, pp. 3133–3174, 2019.
- [32] F.-A. Croitoru, V. Hondru, R. T. Ionescu, and M. Shah, "Diffusion models in vision: A survey," *IEEE Transactions on Pattern Analysis and Machine Intelligence*, vol. 45, no. 9, pp. 10 850–10 869, 2023.
- [33] H. Du, R. Zhang, D. Niyato, J. Kang, Z. Xiong, D. I. Kim, X. Shen, and H. V. Poor, "Exploring collaborative distributed diffusion-based ai-generated content (aigc) in wireless networks," *IEEE Network*, vol. 38, no. 3, pp. 178–186, 2024.
- [34] H. Du, R. Zhang, Y. Liu, J. Wang, Y. Lin, Z. Li, D. Niyato, J. Kang, Z. Xiong, S. Cui *et al.*, "Enhancing deep reinforcement learning: A tutorial on generative diffusion models in network optimization," *IEEE Communications Surveys & Tutorials*, 2024.
- [35] H. Touvron, T. Lavril, G. Izacard, X. Martinet, M.-A. Lachaux, T. Lacroix, B. Rozière, N. Goyal, E. Hambro, F. Azhar *et al.*, "Llama: Open and efficient foundation language models," *arXiv preprint arXiv:2302.13971*, 2023.
- [36] S. Yu, X. Chen, Z. Zhou, X. Gong, and D. Wu, "When deep reinforcement learning meets federated learning: intelligent multitimescale resource management for multiaccess edge computing in 5g ultradense network," *IEEE Internet of Things Journal*, vol. 8, no. 4, pp. 2238–2251, 2021.
- [37] V. Farhadi, F. Mehmeti, T. He, T. F. La Porta, H. Khamfroush, S. Wang, K. S. Chan, and K. Poularakis, "Service placement and request scheduling for data-intensive applications in edge clouds," *IEEE/ACM Transactions on Networking*, vol. 29, no. 2, pp. 779–792, 2021.
- [38] L. Gu, D. Zeng, J. Hu, B. Li, and H. Jin, "Layer aware microservice placement and request scheduling at the edge," in *IEEE INFOCOM 2021-IEEE Conference on Computer Communications*. IEEE, 2021, pp. 1–9.
- [39] W. Chu, P. Yu, Z. Yu, J. C. Lui, and Y. Lin, "Online optimal service selection, resource allocation and task offloading for multi-access edge computing: A utility-based approach," *IEEE Transactions on Mobile Computing*, vol. 22, no. 7, pp. 4150–4167, 2023.
- [40] P. Esser, S. Kulal, A. Blattmann, R. Entezari, J. Müller, H. Saini, Y. Levi, D. Lorenz, A. Sauer, F. Boesel *et al.*, "Scaling rectified flow transformers for high-resolution image synthesis," in *Forty-first International Conference on Machine Learning*, 2024.
- [41] Replicate Platform: <https://replicate.com/>.
- [42] Deepinfra Platform: <https://deepinfra.com/>.
- [43] Stability.AI Platform: <https://stability.ai/>.



Changfu Xu (Student Member, IEEE) received the B.S. degree in Communication Engineering and the M.S. degree in Software Engineering from Jiangxi University of Finance and Economics in 2015 and 2018, respectively. He is currently pursuing a Ph.D. degree in Computer Science and Technology from BNU–HKBU United International College and Hong Kong Baptist University. His main research interests include edge computing and AIGC. He has published more than 10 papers. He won the Best Paper Runner-up Award of IEEE/ACM IWQoS 2024.



Wentao Fan (Senior Member, IEEE) received the M.Sc. and Ph.D. degrees in electrical and computer engineering from Concordia University, Montreal, QC, Canada, in 2009 and 2014, respectively. He is currently an Associate Professor with the Department of Computer Science, Beijing Normal University–Hong Kong Baptist University United International College, Zhuhai, Guangdong, China. He has published more than 100 publications in several prestigious peer-reviewed journals and international conferences. His research interests include machine learning, computer vision, and pattern recognition.



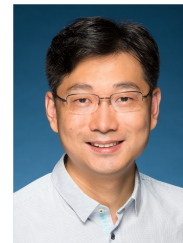
Jianxiong Guo (Member, IEEE) received his Ph.D. degree from the Department of Computer Science, University of Texas at Dallas, Richardson, TX, USA, in 2021, and his B.E. degree from the School of Chemistry and Chemical Engineering, South China University of Technology, Guangzhou, China, in 2015. He is currently an Associate Professor with the Advanced Institute of Natural Sciences, Beijing Normal University, and the Guangdong Key Lab of AI and Multi-Modal Data Processing, BNU–HKBU United International College, Zhuhai, China. He is a member of IEEE/ACM/CCF. He has published more than 80 papers and has been a reviewer in famous international journals/conferences. His research interests include social networks, algorithm design, data mining, IoT applications, blockchain, and combinatorial optimization.



Tian Wang (Senior Member, IEEE) received his BSc and MSc degrees in Computer Science from Central South University in 2004 and 2007, respectively. He received his Ph.D. degree in Computer Science from the City University of Hong Kong in 2011. Currently, he is a professor at the Institute of Artificial Intelligence and Future Networks, Beijing Normal University. His research interests include Internet of Things, edge computing, and mobile computing. He has 30 patents and has published more than 200 papers in high-level journals and conferences. He was a co-recipient of the Best Paper Runner-up Award of IEEE/ACM IWQoS 2024. He has more than 15000 citations, according to Google Scholar. His H-index is 71.



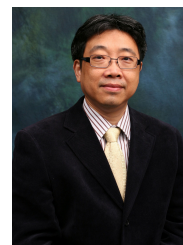
Wanyu Lin (Member, IEEE) received the B.Eng. degree from the School of Electronic Information and Communications, Huazhong University of Science and Technology, Wuhan, China, in 2012, the M.Phil. degree from the Department of Computing, The Hong Kong Polytechnic University, Hong Kong, in 2015, and the Ph.D. degree from the Department of Electrical and Computer Engineering, University of Toronto, Toronto, ON, Canada, in 2020. Her research interests include AI for science and trustworthy machine learning. Dr. Lin has served as an Associate Editor for IEEE TRANSACTIONS ON NEURAL NETWORKS AND LEARNING SYSTEMS.



Xiaowen Chu (Fellow, IEEE) received the B.Eng. degree in computer science from Tsinghua University, Beijing, China, in 1999, and the Ph.D. degree in computer science from The Hong Kong University of Science and Technology, Hong Kong, in 2003. He is currently a Full Professor and Head of Data Science and Analytics Thrust at The Hong Kong University of Science and Technology (Guangzhou). His research interests include GPU Computing, Distributed Machine Learning, Cloud Computing, and Wireless Networks. He has won six Best Paper Awards at different international conferences, including IEEE INFOCOM 2021. He has published over 240 research articles at international journals and conference proceedings. He has served as an associate editor or guest editor of IEEE Transactions on Cloud Computing, IEEE Transactions on Network Science and Engineering, IEEE Transactions on Big Data, IEEE IoT Journal, IEEE Network, IEEE Transactions on Industrial Informatics, etc.



Haodong Zou (Student Member, IEEE) received the B.S. degree in Software Engineering and the M.S. degree in Computer Science and Technology from Anhui University, China, in 2018 and 2021, respectively. He is currently pursuing the Ph.D. degree in Computer Science and Technology from the BNU–HKBU United International College and Hong Kong Baptist University. His main research interests include 5G mobile communication, edge computing and edge intelligence.



Jiannong Cao (Fellow, IEEE) received the B.Sc. degree in computer science from Nanjing University, China, in 1982, and the M.Sc. and Ph.D. degrees in computer science from Washington State University, USA, in 1986 and 1990, respectively. He is currently the Otto Poon Charitable Foundation Professor in data science and the Chair Professor of distributed and mobile computing with the Department of Computing, Hong Kong Polytechnic University, Hong Kong. He is also the Director of the Internet and Mobile Computing Lab at the Department and the Associate Director of the University Research Facility in big data analytics. His research interests include parallel and distributed computing, wireless networks and mobile computing, big data and cloud computing, pervasive computing, and fault-tolerant computing. He has coauthored five books in Mobile Computing and Wireless Sensor Networks, co-edited nine books, and published over 600 papers in major international journals and conference proceedings. He is a Distinguished Member of ACM and a Senior Member of the China Computer Federation (CCF).